Formation of ion-irradiation-induced atomic-scale defects on walls of carbon nanotubes

A. V. Krasheninnikov,[1,2] K. Nordlund,[2] M. Sirviö,[2] E. Salonen,[2] and J. Keinonen[2]
[1]*Moscow State Engineering Physics Institute (Technical University), Kashirskoe shosse 31, 115409 Moscow, Russia*
[2]*Accelerator Laboratory, P.O. Box 43, FIN-00014 University of Helsinki, Finland*
(Received 17 January 2001; published 31 May 2001)

Recent experiments on irradiated carbon nanotubes provide evidence that ion bombardment gives rise to nanotube amorphization and dramatic dimensional changes. Using an empirical potential along with molecular dynamics, we study structure and formation probabilities of atomic-scale defects produced by low-dose irradiation of nanotubes with Ar ions. For this, we simulate impact events over a wide energy range of incident ions. We show that the maximum damage production occurs for a bombarding ion energy of about 600 eV, and that the most common defects produced at all energies are vacancies, which at low temperatures are metastable but long-lived defects. Employing the tight-binding Green's function technique, we also calculate scanning tunneling microscopy (STM) images of irradiated nanotubes. We demonstrate that irradiation-induced defects may be detected by STM and that isolated vacancies may look like bright spots in atomically resolved STM images of irradiated nanotubes.

DOI: 10.1103/PhysRevB.63.245405 PACS number(s): 81.07.De, 61.48.+c, 61.80.Jh, 73.22.−f

I. INTRODUCTION

Unusual mechanical and unique electronic properties of carbon nanotubes (NT's) can be used in numerous applications and can provide ample opportunity for fabricating nanoscale devices (see, e.g., Refs. 1). However, implementation of such devices demands a thorough understanding of the structural and electronic properties not only of perfect NT's, but also of NT's with various atomic-scale defects. Such imperfections may be either created at the time of NT growth[2] or may be induced as a result of external influences such as mechanical strain[3,4] or irradiation[5–7] while the device is in operation. Examples of defects in NT's are pentagon/heptagon Stone-Wales (SW) defects[8] associated with a rotation of a bond in the NT atom network, adatoms on the walls of NT's,[2] and defects initiated through the adsorption of a carbon dimer on a nanotube wall.[2,9]

The issue of how atomic-scale defects influence the structural and electronic properties of NT's has been addressed recently[9–13] with particular focus on the effects on transport properties,[9,13] given the potential application of NT's as quantum wires and field-emission electron guns. The mechanisms of defect formation in NT's under mechanical strain have been studied as well. It has been found that external strain gives rise to atomic restructuring and fourfold carbon rings,[3] as well as to the formation of topological defects,[4] the simplest of which are SW defects, and that NT's release excess strain via a reversible formation of defects.

Studies on the response of NT's to irradiation are also reported, which are of particular importance to understanding the mechanisms of defect development, since irradiation of NT's with electrons, neutrons, or noble-gas ions potentially makes it possible to create defects in a controllable way.

However, theories on the formation of defects in NT's under irradiation and on the subsequent defect evolution over time are far from completion. For instance, one of the unresolved issues is the type and the behavior of irradiation-induced defects in NT's.

Recent experiments[6] evidence that NT's exposed to focused electron irradiation are severely locally deformed and develop necklike features along their bodies due to the removal of carbon atoms by knock-on displacements. Uniform irradiation of NT's also results[5] in surface reconstruction and drastic dimensional changes, as a corollary of which the apparent diameter of NT's shrinks from ≈ 1.4 to 0.4 nm. Tight-binding (TB) molecular dynamics simulations[5] conducted at a temperature of 700 K indicate that irradiation-induced vacancies on NT walls are unstable under high beam dose (when a large number of atoms are removed very rapidly) and at high temperatures. A mending of vacancies occurs through dangling bond saturation and by forming nonhexagonal rings and SW defects, all of which gives rise to surface reconstruction and diameter reduction. However, it is not clear from this work whether single vacancies also transform easily at low temperatures.

On the other hand, although experiments[7] on the interaction of NT's with Ar ion beams also indicate that ion bombardment gives rise to amorphization of NT's and shrinkage of their diameters, appearances of surface dangling bonds in irradiated NT's are reported.[7] Since dangling bonds are usually associated with isolated vacancies, such vacancies, even if metastable, may be long-lived defects (and may survive for macroscopic times), especially under low-temperature, low-dose irradiation.

In this paper, we study the irradiation of individual single-wall NT's with Ar ions. Making use of an empirical potential along with molecular dynamics, we model the impact events as well as the subsequent evolution of the system. We show that single vacancies on NT walls are the predominant defects under low-energy ion irradiation. These defects are stable for our simulation times, at least at room temperatures.

Since scanning tunneling microscopy (STM) probably remains the only tool to identify atom-scale defects directly and since understanding the underlying physics of imperfect

NT's is not possible without determining the type of defects, we also simulate STM images of irradiated NT's within the framework of a TB approach. We demonstrate that irradiation-induced defects may be detected by STM and that, at low bias voltages, vacancies appear as bright spots in STM images due to growth in the local electron density of states on atoms surrounding the vacancy. Electronic superstructures similar to those in graphite near point defects are evident in our theoretical STM images. It should be noted, however, that although atomic resolution has been achieved in a number of experimental works[14,15] we are unaware of signatures of atomic-scale defects having been observed in experimental STM images of NT's.

II. MOLECULAR DYNAMICS SIMULATIONS

We dwell upon (10,10) armchair single-wall NT's, which are assumed to be the predominant constituents of ropes synthesized by the electric arc technique using a catalyst.[16] We stress, however, that our results are qualitatively correct for NT's of different chiralities. We model a portion of long (up to $1\mu m$) *individual* NT's which are also observed experimentally.[5] To avoid excessive computational efforts and to prevent NT's from being displaced by the transfer of momentum, only atoms at a distance of less than 50 Å from the impact point were allowed to move during the relaxation of the atomic structure after ion impact. In actuality, in the TB simulation the 100 Å long nanotubes were augmented by much longer ideal tubes to avoid size-quantization effects.

To simulate defect production by irradiation of NT's, we used classical molecular dynamics. This is the only method fast enough both for realistic simulation of energetic collisional processes and for achieving representative statistics. To model carbon-carbon interaction in the NT, we used the Brenner II interatomic potential, which is constructed to give a good description of vacancies and bond stretching in graphite layers.[17] A good correlation between the results of *ab initio* and classical simulations of NT's is also reported.[2,4] Because bond conjugation is not expected to be significant in the collisional processes, we neglected the computationally intensive four-body part of the potential. To realistically model energetic collisions, we smoothly joined a repulsive potential calculated by a density-functional theory method[19] to the Brenner potential at short interatomic separations.[20] The interaction between Ar and C was modeled with the Ziegler-Biersack-Littmark universal repulsive potential.[21]

In practice, we employed our simulation code, which has previously been used to model irradiation effects in a wide range of metals, semiconductors and carbon-based materials.[22–24] The code uses the Gear V algorithm[25] to integrate the equations of motion and a variable time step dependent on the maximum velocity and interaction force in the system[26] to ensure energy conservation when energetic particles are present in the system. A combined link-cell method and neighbor list is used to achieve linear scaling of the simulation time with the number of atoms.

We first tested the energetics of single vacancies (which have three dangling bonds) and two vacancy-related defects described in Ref. 5. Those defect structures are single-pentagon–one-dangling-bond atomic configurations and fourfold-coordinated atoms in the center of two pentagons and two hexagons. For brevity, we label the former defect ''5-1db'' and the latter the ''5-6'' defect. To calculate the energy, we used the TB[27] and empirical potential models (Brenner potential,[17] Brenner potential without the bond conjugation term, and the original Tersoff potential[18]).

Since we are primarily interested here in the relative stability of the vacancy-related defects, we compare the total energy differences (at 0 K) between the single vacancy and the vacancy-related defects. We find that the 5-1db defect lies 1.8, 3.0, 0.9, and -1.0 eV below (above for negative signs) the single vacancy in energy for the tight-binding, full Brenner potential, Brenner potential without the bond conjugation term, and the original Tersoff potential, respectively. Our results for the 5-6 defect are -0.4, 2.4, 0.9, and -1.3 eV below the single vacancy for the same potentials. The energy differences do depend heavily on the theoretical models used. However, since it is known that it is very difficult to calculate the formation energies of vacancylike defects in covalent systems even with density-functional methods,[28] we think that no more than a qualitative agreement can in any case be desired at this stage. Since both the results of Ajayan *et al.*[5] and our better models (TB and Brenner) all predict that the 5-1db defect is lowest in energy, this provides strong evidence that this is the most stable missing-atom defect configuration in nanotubes.

To simulate Ar impacts on the NT, we shot an Ar ion placed well outside the tube toward the center of the tube. The impact point was chosen randomly, and the Ar ion shot toward the central axis of the tube. Between 40 and 170 ions were simulated at different energies to obtain reasonably small statistical uncertainties in the main quantities calculated. The simulation was carried out for 5 ps per event using temperature scaling only at the outer edges of the NT (where no collisional processes took place). Defects were detected by visual inspection of the final atom positions.

To examine the stability of the vacancies, we simulated a single vacancy in a 100 Å long nanotube with no fixed atoms over time scales up to more than ten nanoseconds at temperatures of 500–4000 K. We found that at high temperatures a single vacancy does transform into the same 5-6 configuration and 5-1db configuration observed in Ref. 5 and becomes mobile. At least at temperatures below 2500 K, the clearly dominant process was a transformation into the 5-1db defect, as expected from the defect energetics. With simulations between temperatures of 1500 K and 2200 K, we determined that the average vacancy lifetime can be well described with activated behavior with a single activation energy, i.e., by the formula $\tau = a\exp(b/k_BT)$, where τ is the time before the vacancy transforms into something else, k_B is Boltzmann's constant, T is the temperature, and a and b are the fitting constants. Our best fit gave $a = 0.18 \pm 0.02$ ps and $b = 1.2 \pm 0.1$ eV.

Since the TB and classical models give dissimilar energy differences for the defects (see above), it is clear that each model can be expected to give a somewhat different activation energy as well. We note, however, that the initial part of the transformation from the vacancy to any other structure

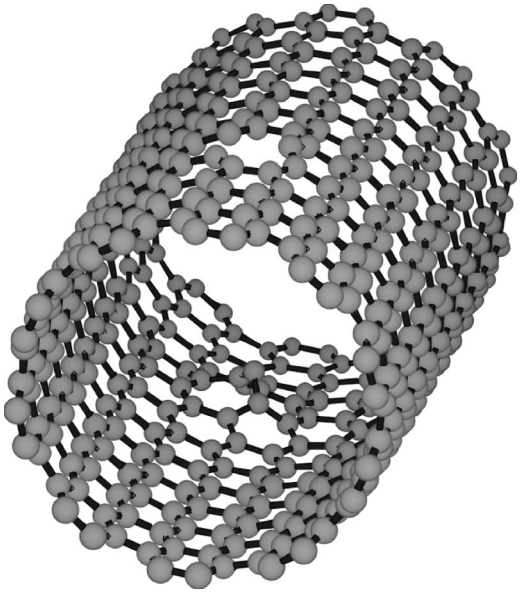

FIG. 1. Ball-and-stick representation of a (10,10) NT after ion impact and subsequent relaxation. A vacancy is evident in the upper part of the NT and a carbon knocked-off atom adsorbed inside the NT in a D3 configuration is also observable.

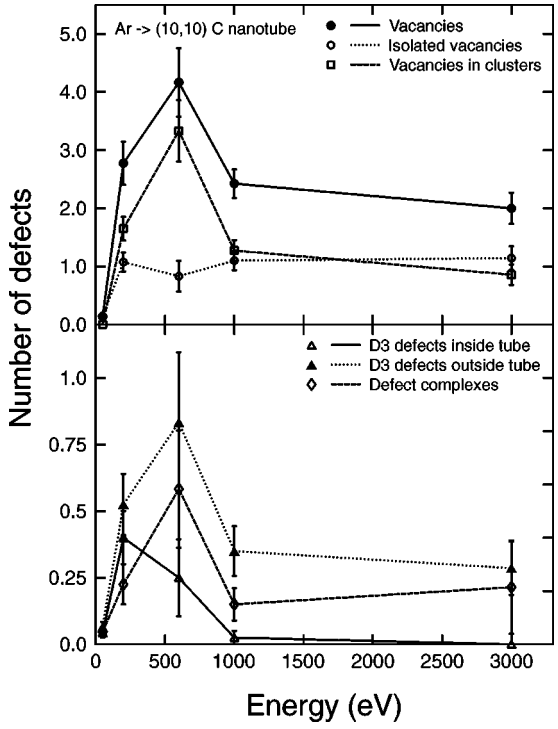

FIG. 2. Average number of defects formed for one bombarding Ar ion as a function of the ion energy. The upper part shows the formation probabilities of vacancy-type defects, the lower part other defects. Note the difference in the ordinate scales.

involves an elastic stretching of bonds. Since the Brenner II potential describes bond stretching well, it can thus be expected to give a good description of at least the lower part of the energy barrier separating different defect configurations.

We also studied the stability of isolated vacancies in NT's using a TB approach, which has been proven to be very reliable in calculating structural and electronic properties of NT's.[9–13] We used the parametrization of the TB Hamiltonian suggested in Ref. 27. We found that isolated vacancies were quite stable for the entire duration of our TB molecular dynamics simulations (about 5 ps) even at temperatures exceeding 1000 K. However, at 2000 K we observed formation of 5-1db defects during our simulations.

Thus, both the classical and TB models indicate that at low temperatures the vacancy is stable on long time scales. If the activation energy for vacancy transformation is $\gtrsim 1$ eV, as our simulations indicate, the vacancies can be expected to be stable at room temperature for time scales of at least the order of hours. Thus, they might be experimentally found.

A typical defect configuration which appeared in a (10,10) NT after ion impact and the subsequent relaxation of carbon network is represented in Fig. 1. A vacancy is evident in the upper part of the NT, whereas in the lower part a carbon knocked-off atom is adsorbed on the wall inside the NT.

Twofold-coordinated single adatoms on both external and internal sides of the NT walls are also prolific after ion impact. Defects of this type for graphite have been previously labeled[20] ''D3,'' so, in what follows, we use this term as well. The geometry of D3 defects (bond lengths and angles) are very close to those reported in Ref. 20. We found that such defects are stable at low temperatures. Recent simulations[2] also show that D3 defects can survive even when the NT is annealed at 3000 K. Other complex defects (clustered vacancies, non-hexagonal rings, etc.) appear after ion impact as well. However, we have never observed any defect structures that might be labeled as in-plane interstitials in the NT. This is not unexpected, as an extra carbon atom lying in a graphitelike plane would need to have either an unnaturally high number of bonds or prohibitively short ones. Thus, we reach the conclusion that the D3 defect can be expected to be the predominant interstitial-like defect produced in nanotubes during irradiation.

The production of different varieties of defects as a function of incident ion energy is illustrated in Fig. 2. That figure shows the average number of defects produced for different energies of the bombarding Ar ion (50, 200, 600, 1000, and 3000 eV). The upper half shows the total number of vacancies produced, as well as how this number is divided into isolated vacancies and vacancies in clusters. The lower half shows the number of D3 defects where the adatom is inside or outside the tube. Also shown is the number of defect complexes, i.e., defect structures that could not be classified into any of these simple categories.

Note that the difference in the ordinate scale is about a factor of 5 in the two parts of the figures. This shows that the dominant type of defects produced during heavy-ion irradiation of NT's is always a vacancy. At the very lowest energy (50 eV), monovacancies dominate because this energy is so close to the defect production threshold that it is highly unlikely that complex defects could form. At intermediate energies, vacancies that are in clusters of at least two vacancies dominate and at higher energies (>1 keV) the number of monovacancies and vacancies in clusters is about the same.

Figure 2 shows that for all defect types except D3 defects inside the tube, the maximum in damage production occurs at about 600 eV. The damage production increases between 50 and 600 eV simply because there is more energy available for it. At higher ion energies, defect production decreases as the nuclear collision cross section decreases, making defect-producing collisions less likely.

To estimate the possible model dependency of the results, we also simulated 200 eV Ar bombardment events with the Brenner potential, which includes bond conjugation effects. We found that the number of monovacancies was the same within the uncertainties, while the other defect numbers (D3 defects and clustered vacancies) were $\sim 50\%$ lower. Since monovacancies can be produced by a single ballistic collision, it is not surprising that their amount is similar. The number of the other defects apparently is more sensitive to the detailed nature of the atomic interaction. Our main objective here is to examine how the damage production qualitatively changes with energy, which will be largely governed by how much energy is transferred in initial ballistic collisions from Ar to the C network. Hence, although the choice of the potential clearly affects the absolute numbers somewhat, the overall energy dependence can be expected to be insensitive to the choice of the potential.

III. TIGHT-BINDING SIMULATIONS OF STM IMAGES OF IRRADIATED NANOTUBES

Having used classical molecular dynamics to calculate an event of an Ar ion impact on the NT and subsequent relaxation of the carbon network, we computed the STM images of the irradiated NT's within the framework of the TB approximation. Our technique has been successfully used for calculations of STM images of graphite surfaces with point defects[29] and NT's,[30] the latter being treated within the framework of a simple nearest-neighbor TB model. Since the electronic structure of single-wall NT's near the Fermi energy is governed by the π states oriented perpendicularly to the NT walls, in our simulation, we employed a one-band TB Hamiltonian that accounts for electron hopping beyond the first-neighbor approximation. To account for the dependence of the hopping elements on interatomic distances, we used the scaling functions given in Ref. 27.

The STM tip was modeled as the final atom of a semi-infinite, one-dimensional chain. To the first order in the tip-NT interaction, which was treated perturbatively, the tunneling current I as a function of the tip coordinates (x,y,z) may be written[31] at zero temperature as

$$I(x,y,z) = \frac{2\pi e}{\hbar} \int_{E_F}^{E_F + eV_{\text{bias}}} \sum_i |V_i(x,y,z)|^2 \rho_{\text{tip}}(E) \rho_{\text{tube}}(i,E) dE, \quad (1)$$

where the sum runs over all sites involved in the tip-NT hopping. V_{bias} is the bias voltage applied to the tip-NT interface, $V_i(x,y,z)$ is the tunneling matrix element coupling the tip apex atom to the atom i of the NT, $\rho_{\text{tip}}(E)$ and $\rho_{\text{tube}}(i,E)$ are the local densities of states (LDOS's) of the noninteracting tip and the NT, respectively. The parameter V was evaluated numerically with the tip states being approximated by a hydrogenlike d function mimicking a tungsten tip.

Note that Eq. (1) has an approximate character: it involves densities of states of the nanotube and tip only, but not off-diagonal elements of the nanotube and tip Green's functions, as needed in a strict tight-binding formulation of STM. However, if the separation between the nanotube and tip is more than 4 Å (and we chose a value of the reference current in such a way that this condition was met), this formula works very well for carbon systems.[31]

The recursion method[32] was employed to calculate the LDOS of a nanotube. STM images were computed for the constant current mode of STM operation, in which the height of the STM tip is adjusted to keep a constant value of current. To simulate this mode, we numerically solved the Eq. (1) for the z coordinate (tip height $h \equiv z$) at any scan point (x,y).

In our calculations, we ignored the mechanical deformation of the surface induced by the STM tip, as well as any possible Ohmic contacts appearing due to contamination of the STM tip as a result of working with carbonaceous materials.[33] A small $V_{\text{bias}} = \pm 0.2$ V was considered. Thus, only electronic states near E_F contribute to the tunneling current. We account for the shift[14] of E_F by $\delta E = 0.3$ eV due to the charge transfer from the substrate, which leads to an asymmetric position of the NT band structure relative to E_F, see Fig. 4(b).

Figure 3(a) schematically illustrates the image formation mechanism: tip height $h \equiv z$ as a function of tip position for a scan in a direction perpendicular to the tube axis is shown. The isometric plot of h as a function of tip position in the (x,y) plane is represented in Fig. 3(b) for the NT shown in Fig. 1 and for $V_{\text{bias}} = +0.2$. The vacancy is at the origin. All lengths are given in Ångstroms. The central part of the image corresponding to the topmost part of the NT (-5 Å $< y < 5$ Å) is shown. A dramatic hillocklike feature above the vacancy is evident. The height of the protrusion constitutes ≈ 1 Å, while its linear size is about 10 Å. To achieve atomic corrugation, we subtract the profile of the NT averaged over its axis from the initial profile; see Fig 3(c). Figures 3(d) and 3(e) depict the filtered STM images of the central part of the NT. The shape of the hillock is governed by that of the atoms in the NT carbon network.

To understand the origin of the hillock, in Fig. 4(a) we plot the current-to-voltage (I-V) characteristic for the tip positioned above the vacancy. The I-V curve is actually the LDOS on carbon atoms surrounding the vacancy and contributing to the tunneling current. In Fig. 4(b) we plot the I-V curve calculated at a distance from the vacancy, and this coincides with the I-V curve for a defect-free NT. As it is evident from the figures, the vacancy results in a sharp increase in LDOS near E_F on atoms nearest the vacancy. This increase stems from the states close to the E_F spatially localized on atoms near the vacancy, which may be also interpreted as dangling bonds. Since it is specifically these states that STM probes at small bias voltages, a vacancy is imaged as a protrusion. A similar effect has been reported for surface vacancies in graphite, see Refs. 20 and 29 and references therein.

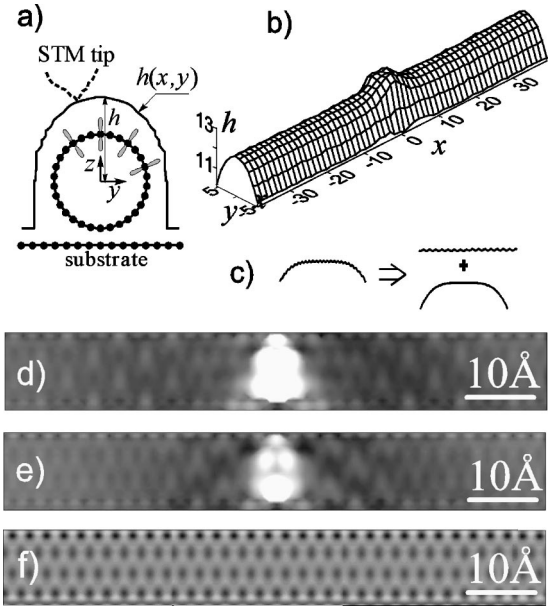

FIG. 3. STM image of a (10,10) irradiated NT. (a) Schematic plot of tip height h as a function of tip position for a scan in a direction perpendicular to the tube axis. (b) Isometric plot of h as a function of tip position in the (x,y) plane for $V_{\text{bias}}=+0.2$. (c) Illustration for achieving atomic corrugation (''filtering'' the STM image) by subtracting the averaged (over the NT axis x) profile of the nanotube. (d) and (e) Gray-scale ''filtered'' STM images of the irradiated NT for positive and negative values of V_{bias}, respectively. The vacancy is at the origin in the (x,y) plane (at the centers of the images). (f) Gray-scale ''filtered'' STM image of a (10,10) NT without defects.

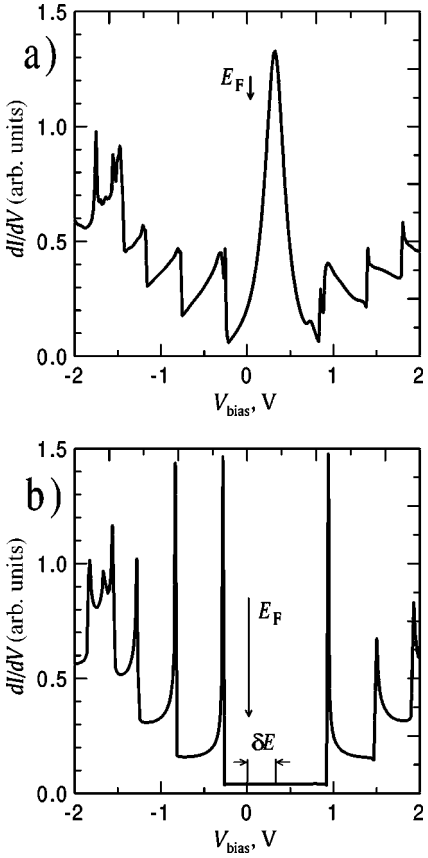

FIG. 4. I-V curves for the (10,10) NT calculated (a) just above the vacancy and (b) above an atom distanced from the defect. The arrow indicates the position of E_F and δE is the shift of E_F due to the charge transfer from the substrate.

Along with a hillocklike feature, it can also be seen from Fig. 3(d) that the STM image of the NT in the vicinity of the vacancy is different from that observed for the defect-free case [given in Fig. 3(f)]. A network of dark spots corresponding to the centers of hexagons (typical for defect-free NT's) is no longer evident, whereas modulations in h along the NT axis are present. However, it is seen that the network of dark spots is gradually restored at the ends of the images.

Since we did not find any rearrangement of NT atoms distanced from the defect after the geometry optimization, these modulations, or superstructures, with a period commensurate with (but larger than) that of the underlying graphene lattice also stem from electronic effects: periodic modulations in the LDOS on carbon atoms in the vicinity of the vacancy. Our simulation confirm predictions[34] on the anisotropy of STM images near point defects on NT walls and specify the shape of superstructures resulting from irradiation-induced small-scale defects.

We also calculated STM images near other defects. As expected, D3 defects on the *external* side of the NT walls appear as very sharp protrusions due to the geometry of these defects. However, experimentally observing them is hardly possible since D3 defects are likely to be picked up and transposed by the STM tip. D3 defects on the *internal* side of the NT walls could be detected by STM. Within our model, they look like small hillocks due to the local increase in the LDOS. However, the height of D3-induced hillocks is much less than the height of those induced by vacancies.

IV. CONCLUSIONS AND OUTLOOK

In this paper, we simulated the irradiation of NT's with 50–3000 eV Ar ions using empirical potential molecular dynamics to study the structure and formation probabilities of atomic-scale defects produced by low-dose irradiation of NT's. In order to juxtapose our results to possible experimental signatures of such defects in NT's, we also employed the tight-binding Green's-function technique to calculate STM images of irradiated NT's.

We showed that low-dose irradiation results in the formation of various atom-scale defects on NT walls and that the maximum damage production occurs for a bombarding ion energy of roughly 600 eV. The most common defects produced at all energies are vacancies, and at low temperatures isolated vacancies are metastable, but long-lived, defects. At the same time, annealing the NT's at high temperatures and irradiating them with high doses probably leads to vacancy mending via dangling bond saturation.

Irradiation-induced defects may be detected by STM and isolated vacancies may appear as bright spots in atomically resolved STM images of irradiated NT's analogous to experimental STM images of graphite surfaces with

vacancies.[35,36] Electronic superstructures similar to those[35] in graphite near point defects are evident in our theoretical STM images.

Since vacancies in NT's, unlike vacancies in graphite, seem to be metastable, real-time atomic-resolution STM probing of irradiated NT's may enable one to observe the temporal evolution of such irradiation-induced defects at various temperatures and compare experimental lifetimes to those predicted theoretically. Thus, experiments on irradiating NT's with inert gas ions and subsequent STM probing may not only contribute to understanding the mechanisms of defect formation, but may also serve as a test for the validity of TB and empirical potential molecular dynamics models.

ACKNOWLEDGMENTS

A. V. K. greatly benefited from discussions with V. F. Elesin, L. Openov, and D. Cannon. The research was supported by TEKES under the FFUSION2 program, and the Academy of Finland under Project Nos. 44215 and 73722. Grants of computer time from the Center for Scientific Computing in Espoo, Finland are gratefully acknowledged.

[1] C. Dekker, Phys. Today **52(5)**, 22 (1999); M.S. Dresselhaus, G. Dresselhaus, and P.C. Eklund, *Science of Fullerenes and Carbon Nanotubes* (Academic Press, New York, 1996); *Carbon Nanotubes, Preparation and Properties*, edited by T.W. Ebbesen (CRC, Boca Raton, FL, 1997); P.J. Harris, *Carbon Nanotubes and Related Structures* (Cambridge University Press, Cambridge, 1999); P.M. Ajayan and T.W. Ebbesen, Rep. Prog. Phys. **60**, 1025 (1997); P.M. Ajayan, Chem. Rev. **99**, 1787 (1999); M. Terrones, W.K. Hsu, H.W. Kroto, and D.R.M. Walton, Top. Curr. Chem. **199**, 189 (1999).

[2] Y. Xia, Y. Ma, Y. Xing, Y Mu, C. Tan, and L. Mei, Phys. Rev. B **61**, 11 088 (2000).

[3] M.S.C. Mazzoni and H. Chacham, Phys. Rev. B **61**, 7312 (2000).

[4] M. B. Nardelli, B.J. Yakobson, and J. Bernholc, Phys. Rev. B **57**, 4277 (1998).

[5] P.M. Ajayan, V. Ravikumar, and J.-C. Charlier, Phys. Rev. Lett. **81**, 1437 (1998).

[6] C.-H. Kiang, W.A. Goddard, R. Beyers, and D.S. Bethune, J. Phys. Chem. **100**, 3749 (1996).

[7] Y. Zhu, T. Yi, B. Zheng, L. Cao, Appl. Surf. Sci. **137**, 83 (1999).

[8] A.J. Stone and D.J. Wales, Chem. Phys. Lett. **73**, 122 (1986).

[9] D. Orlikowski, M.B. Nardelli, J. Bernholc, and C. Roland, Phys. Rev. B **61**, 14 194 (2000).

[10] A. Rubio, Appl. Phys. A: Mater. Sci. Process. **68**, 275 (1999).

[11] V. Meunier and Ph. Lambin, Carbon **38**, 1729 (2000).

[12] J.-C. Charlier, T.W. Ebbesen, and Ph. Lambin, Phys. Rev. B **53**, 11 108 (1996).

[13] L. Chico, L.X. Benedict, S.G. Louie, and M.L. Cohen, Phys. Rev. B **54**, 2600 (1996); A. Hansson, M. Paulsson, and S. Stafström, *ibid.* **62**, 7639 (2000); M. Igami, T. Nakanishi, and T. Ando, Physica B **284-288**, 1746 (2000); H.J. Choi, J. Ihm, S.G. Louie, and M.L. Cohen, Phys. Rev. Lett. **84**, 2917 (2000); T. Kostyrko, M. Bartkowiak, and G.D. Mahan, Phys. Rev. B **60**, 10 735 (1999).

[14] L.C. Venema, J.W. Janssen, M.R. Buitelaar, J.W.G. Wildöer, S.G. Lemay, L.P. Kouwenhoven, and C. Dekker, Phys. Rev. B **62**, 5238 (2000).

[15] J.W.G. Wildöer, L.C. Venema, A.G. Rinzler, R.E. Smalley, and C. Dekker, Nature (London) **391**, 59 (1998); T.W. Odom, J.L. Huang, P. Kim, and C.M. Lieber, *ibid.* **391**, 62 (1998); A. Hassanine, M. Tokumoto, Y. Kumazawa, H. Kataura, Y. Maniwa, S. Suzuki, and Y. Achiba, Appl. Phys. Lett. **73**, 3839 (1998).

[16] C. Journet, W.K. Maser, P. Bernier, A. Loiseau, M. Lamy de la Chapelle, S. Lefrant, P. Deniard, R. Lee, and J.E. Fischer, Nature (London) **388**, 756 (1997).

[17] D.W. Brenner, Phys. Rev. B **42**, 9458 (1990).

[18] J. Tersoff, Phys. Rev. Lett. **61**, 2879 (1988).

[19] K. Nordlund, N. Runeberg, and D. Sundholm, Nucl. Instrum. Methods Phys. Res. B **132**, 45 (1997).

[20] K. Nordlund, J. Keinonen, and T. Mattila, Phys. Rev. Lett. **77**, 699 (1996).

[21] J.F. Ziegler, J.P. Biersack, and U. Littmark, *The Stopping and Range of Ions in Matter* (Pergamon, New York, 1985).

[22] K. Nordlund, M. Ghaly, R. S. Averback, M. Caturla, T. Diaz de la Rubia, and J. Tarus, Phys. Rev. B **57**, 7556 (1998).

[23] K. Nordlund, J. Nord, J. Frantz, and J. Keinonen, Comput. Mater. Sci. **18**, 283 (2000).

[24] E. Salonen, K. Nordlund, J. Keinonen, and C.H. Wu, Europhys. Lett. **52**, 504 (2000).

[25] G. Gear, *Numerical Initial Value Problems in Ordinary Differential Equations* (Prentice-Hall, Englewook Cliffs, NJ, 1971).

[26] K. Nordlund, Comput. Mater. Sci. **3**, 448 (1995).

[27] C.H. Xu, C.Z. Wang, C.T. Chan, and K.M. Ho, J. Phys.: Condens. Matter **4**, 6047 (1992).

[28] M.J. Puska, S. Pöykko, M. Pesola, and R.M. Nieminen, Phys. Rev. B **58**, 1318 (1998).

[29] A.V. Krasheninnikov and V.F. Elesin, Surf. Sci. **454-456**, 519 (2000).

[30] A.V. Krasheninnikov, Phys. Low-Dimens. Semicond. Struct. **11/12**, 1 (2000); A.V. Krasheninnikov, Solid State Commun. **118**, 361 (2001).

[31] B.A. McKinnon and T.C. Choy, Phys. Rev. B **54**, 11 777 (1996).

[32] R. Haydoc, Sov. J. Plasma Phys. **35**, 216 (1980); C.M. Goringer, D.R. Bowler, and E. Hernández, Rep. Prog. Phys. **60**, 1447 (1997).

[33] F.-X. Zha, R. Czerw, D.L. Carroll, Ph. Kohler-Redlich, B.-Q. Wei, A. Loiseau, and S. Roth, Phys. Rev. B **61**, 4884 (2000).

[34] C.L. Kane and E.J. Mele, Phys. Rev. B **59**, R12 759 (1999).

[35] J.R. Hahn and H. Kang, Phys. Rev. B **60**, 6007 (1999).

[36] J.G. Kushmerick, K.F. Kelly, H.-P. Rust, N.J. Halas, and P.S. Weiss, J. Phys. Chem. B **103**, 1619 (1999).